JCTC Journal of Chemical Theory and Computation

Quantum Chemical Benchmark Studies of the Electronic Properties of the Green Fluorescent Protein Chromophore: 2. *Cis*−*Trans* Isomerization in Water

Igor Polyakov,[†] Evgeny Epifanovsky,*[,‡] Bella Grigorenko,[†] Anna I. Krylov,*[,‡] and Alexander Nemukhin[†,§]

Department of Chemistry, University of Southern California, Los Angeles, California 90089, Department of Chemistry, M.V. Lomonosov Moscow State University, Moscow 119991, Russia, and Institute of Biochemical Physics, Russian Academy of Sciences, Moscow 119334, Russia

Received March 25, 2009

Abstract: We present quantum chemical calculations of the properties of the anionic form of the green fluorescent protein (GFP) chromophore that can be directly compared to the results of experimental measurements: the *cis*−*trans* isomerization energy profile in water. Calculations of the *cis*−*trans* chromophore isomerization pathway in the gas phase and in water reveal a problematic behavior of density functional theory and scaled opposite-spin-MP2 due to the multiconfigurational character of the wave function at twisted geometries. The solvent effects treated with the continuum solvation models, as well as with the water cluster model, are found to be important and can reduce the activation energy by more than 10 kcal/mol. Strong solvent effects are explained by the change in charge localization patterns along the isomerization coordinate. At the equilibrium, the negative charge is almost equally delocalized between the phenyl and imidazolin rings due to the interaction of two resonance structures, whereas at the transition state the charge is localized on the imidazolin moiety. Our best estimate of the barrier obtained in cluster calculations employing the effective fragment potential-based quantum mechanics/molecular mechanics method with the complete active space self-consistent field description of the chromophore augmented by perturbation theory correction and the TIP3P water model is 14.8 kcal/mol, which is in excellent agreement with the experimental value of 15.4 kcal/mol. This result helps to resolve previously reported disagreements between experimental measurements and theoretical estimates.

1. Introduction

The properties of the green fluorescent protein (GFP), which converts blue light to green light, have inspired numerous experimental and theoretical studies as well as many important applications (see ref 1–3 and references therein). This paper is the second in a series[4] that focuses on accurate calculations of the properties of biological chromophores with ab initio methods using the model GFP chromophore, 4′-hydroxybenzylidene-2,3-dimethylimidazolinone (HBDI) anion, as a benchmark system (Figure 1).

The *cis*−*trans* isomerization (or *Z*/*E* diastereomerization) of the photoswitchable fluorescent chromophores plays an essential role in their photophysical properties. For example, their functionality is believed to be driven by photoinduced *cis*−*trans* isomerization inside a protein matrix.[5] Kindling and blinking phenomena, as well as loss of fluorescence yield of bare chromophores in solution, are also related to this process. In a broader context, the photophysics of GFP is similar to that of other fluorogenic unsymmetric methine

* Corresponding authors. E-mail: epifanov@usc.edu (E.E.) and krylov@usc.edu (A.I.K.).

[†] M.V. Lomonosov Moscow State University.

[‡] University of Southern California.

[§] Russian Academy of Sciences.

10.1021/ct9001448 CCC: $40.75 © 2009 American Chemical Society
Published on Web 06/25/2009

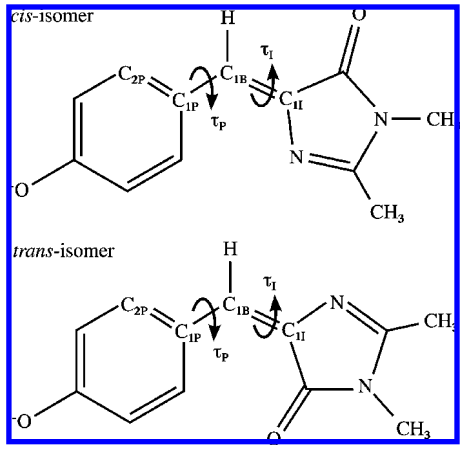

Figure 1. Chemical structure and atomic labels of the anionic form of the model GFP chromophore HBDI in the *cis* (top) and *trans* (bottom) conformations.

dyes[6–11] and is of interest with connection to organic photovoltaic materials.

The majority of the experimental and computational studies of this process focused on the excited-state dynamics. However, the ground-state electronic potential-energy surface (PES) also needs to be considered for two main reasons. First, after photoisomerization has completed, the photoswitchable protein returns to its initial state to prepare for the next cycle. The recovery apparently takes place on the ground-state PES. Second, the details of the ground-state isomerization can elucidate the chromophore's rearrangements along the more complicated excited-state route. Despite previous studies of the *cis*−*trans* photoisomerization of GFP-like chromophores[12–17] using quantum chemistry modeling,[18–24] many questions remain unanswered.

The process of *cis*−*trans* isomerization of the HBDI anion in aqueous solution was investigated experimentally by He et al.[12] who estimated the free-energy differences and the activation energies using the NMR technique. The authors stressed that the activation energy of 15.4 kcal/mol derived from their measurements in aqueous solution is in distinct disagreement with the results of calculations,[18,19] which estimated that the barrier is above 21 kcal/mol. The relatively low value of the barrier (as compared to other isomerization reactions involving exocyclic double bonds) has also been emphasized in subsequent studies of the isomerization and several explanations have been suggested.[13,17] For example, thermal isomerization studies of model GFP-like compounds[13] suggested that different substituent groups may have a significant effect on the activation energy by changing the interaction between two resonance structures of the chromophore. Tolbert and co-workers considered mechanisms involving changes in the chemical structure of the chromophore, e.g., addition/elimination pathway.[17] No ab initio calculations have been reported so far to resolve this disagreement between experimental measurements and theoretical estimates and to explain the low value of the barrier.

2. Computational Methods

The equilibrium geometries were optimized by density functional theory (DFT) with the PBE0 variant[25] of the Perdew−Burke−Ernzerhof (PBE) hybrid functional[26] and by complete active space self-consistent field (CASSCF)(14/12). The cc-pVDZ basis set[27] was used in both calculations. The *cis*−*trans* isomerization pathways of the chromophore were studied with the DFT and CASSCF methods. We estimated the solvent effects by using continuum solvation models as well as by explicit treatment of water molecules in a quantum mechanics/molecular mechanics (QM/MM) scheme. The Cartesian coordinates of optimized structures along the isomerization pathway are given in the Supporting Information.

The methods are outlined below and in the first paper in this series,[4] and the computational details are given in the Results and Discussion section. Multireference second-order perturbation theory (MRMP2) and dielectric polarizable continuum model (D-PCM)[33] calculations were carried out with the PC GAMESS version[28] of the GAMESS(US) quantum chemistry package.[29] Scaled opposite-spin-MP2 (SOS-MP2) calculations were performed with Q-Chem.[30] GAMESS(US)[29] was employed for C-PCM and surface and volume polarization for electrostatic (SVPE) approach[35] computations. The QM/MM implementation is based on PC GAMESS[28] and the Tinker molecular mechanics package.[31]

2.1. Continuum Solvation Models. To simulate solvent effects on the chromophore's *cis*−*trans* isomerization energy profile in an aqueous solution, we employ three versions of the continuum solvation model:[32] D-PCM, C-PCM, and SVPE. In the simplest approach, the D-PCM,[33] the water solvent is treated as a continuous unstructured dielectric with a dielectric constant of 78.39. C-PCM[34] is a version of PCM that takes into account certain corrections in the boundary conditions of the electrostatic problem in accord with the conductor-like screening model. The SVPE approach[35] provides an improved description of the volume polarization contributions. This effect can be significant for reaction barriers, especially for ionic solutes.[35]

2.2. Effective Fragment Potential-Based QM/MM Method. Solvent effects can be described explicitly in a combined QM/MM approach based on the effective fragment potential (EFP) model.[36,37] In this scheme, solvent molecules (water in our case) are represented by effective fragments in the MM-part. The fragments affect the Hamiltonian of the QM-part (HBDI anion) by their electrostatic potentials expanded up to octupole terms. The parameters of these one-electron electrostatic potentials, as well as contributions from interactions between polarizable effective fragments and the QM-region, are computed in preliminary ab initio calculations of the electronic densities of individual fragments. The exchange−repulsion potentials, which are combined with the electrostatic and polarizability terms, are obtained from preliminary ab initio calculations as well.

The original EFP approach[36] treats interactions between solvent molecules as EFP−EFP interactions. Studies of chemical reactions in aqueous solution[38,39] have shown that replacing the EFP−EFP terms by the empirically calibrated TIP3P potential yields a faster computational scheme for large water clusters around the solute.

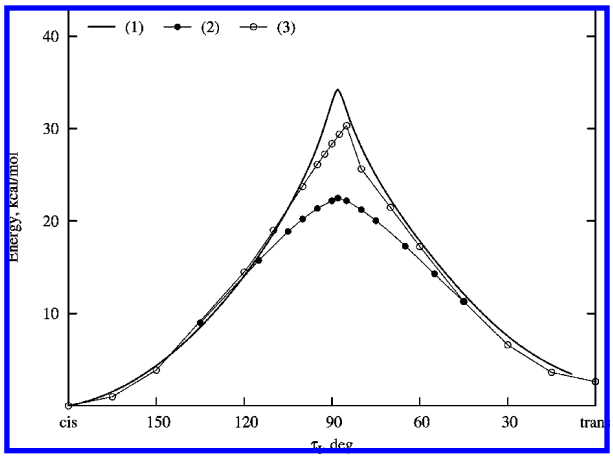

Figure 2. Computed energy profiles of *cis*−*trans* ground-state isomerization of the HBDI anion in the gas phase: (1) IRC calculated with DFT(PBE0)/6-31+G(d,p); (2) MEP calculated with CASSCF(12/11)/cc-pVDZ; and (3) MEP calculated with SOS-MP2/cc-pVDZ.

3. Results and Discussion

3.1. *Cis*−*Trans* Isomerization Pathway in the Gas Phase. On the ground-state PES, conversion between the lower-energy *cis*-isomer and the higher-energy *trans*-isomer takes place when the two rings are rotated along the $C_{1I}-C_{1B}$ bond as shown in Figure 1. The dihedral angle $N-C_{1I}-C_{1B}-H$, which defines the reaction coordinate, is denoted as τ_I.

The shape of the isomerization pathway can be characterized by: (i) the activation energy E_a defined as the relative energy of the transition state (TS) with respect to the *cis*-isomer; and (ii) the energy difference E_{tc} between the *trans*- and *cis*-forms. We began with gas-phase DFT calculations with the PBE0 functional and the 6-31+G(d,p) basis set and located stationary points that correspond to the *cis*-, *trans*- and TS structures. The latter is characterized by a single imaginary frequency of $725i$ cm^{-1}. The intrinsic reaction coordinate (IRC) profile was computed by starting steepest descent pathways from the TS point in both directions along the Hessian eigenvector that corresponds to the imaginary frequency (shown in Supporting Information).

The results of this calculation are discouraging in two aspects: the cusp-like shape of the profile (Figure 2), which is consistent with the large value of the imaginary frequency at the saddle point, and the value of the activation energy E_a(DFT) = 34.5 kcal/mol, which is more than twice as high as the experimental estimate of 15.4 kcal/mol in aqueous solution.[12] The computed energy difference between the *trans*- and *cis*- structures E_{tc}(DFT) = 2.3 kcal/mol is in excellent agreement with the experimental estimate in solution,[12] most likely due to error cancellation.

In the CASSCF energy profile (Figure 2), the stationary points were fully optimized with CASSCF(12/11)/cc-pVDZ. The points in between representing the minimum-energy path (MEP) were computed by varying the value of the dihedral angle τ_I and minimizing the energy by relaxing all other degrees of freedom. Although this curve does not represent the true IRC path, it is expected to be a good approximation to it. Along with a smoother curvature in the vicinity of the saddle point (imaginary frequency $77i$ cm^{-1}, see Supporting Information), this profile yields a reasonable value of the *trans-cis* energy difference E_{tc}(CASSCF) = 3.5 kcal/mol and a much lower (and closer to the experimental estimate) value of the activation energy E_a(CASSCF) = 22.5 kcal/mol.

When calculating the energy profile in the CASSCF(12/11) approximation with a fairly large active space, we performed careful selection of the orbitals in order to avoid dubious solutions of the variational problem. The finally optimized orbitals and the corresponding occupation numbers at selected points along the energy graph are presented in the Supporting Information. To better understand changes in the electronic structure along the isomerization pathway, we also computed the energy profile with the smallest active space CASSCF(2/2). Selection of active orbitals in this approach was performed on the base of previously optimized orbitals at the TS point. Then the descent in both directions toward minimum-energy structures was easy to accomplish. As expected, the corresponding value of the activation energy, 25 kcal/mol, was slightly larger than that computed with CASSCF(12/11).

As discussed in more detail below (and illustrated by the population analysis presented in Supporting Information), there is an increase in charge localization at the TS relative to that the minimum-energy points.

The transition state located with SOS-MP2/cc-pVDZ is characterized by an imaginary frequency of $188i$ cm^{-1}. Starting from that point, the MEP was taken to the *cis*- and *trans*-configurations (Figure 2). Both DFT and SOS-MP2 exhibit a cusp at the transition state, which is a manifestation of the multireference character of the ground-state wave function. The composition of the CASSCF wave function in the region discussed below confirms that.

Table 1 presents computed equilibrium geometry parameters in the bridging region: the $C_{1P}-C_{1B}$ and $C_{1I}-C_{1B}$ bond lengths and the τ_P ($C_{2P}-C_{1P}-C_{1B}-H$) and τ_I ($N-C_{1I}-C_{1B}-H$) dihedral angles (Figure 1). The parameters optimized at the PBE0/6-31+G(d,p), CASSCF(12/11)/cc-pVDZ, and SOS-MP2/cc-pVDZ levels are in agreement with those obtained by Olsen and Smith[23] with SA3-CAS(4/3)/DZP, which stands for CASSCF with the (4/3) active space averaged over three states computed with the DZP basis set. Overall, the geometry parameters at the stationary points are rather insensitive to the level of theory: DFT, large active space state-specific CASSCF, small active space state-averaged CASSCF, and SOS-MP2 yield bond lengths that agree within 0.02 Å and angles that agree within 2°.

At both *cis*- and *trans*-equilibrium points, the molecule is essentially planar except that the methyl groups naturally have out-of-plane atoms. Analysis of the structures reveals that the difference between $C_{1P}-C_{1B}$ and $C_{1B}-C_{1I}$ is less than expected for the structure shown in Figure 1. This can be explained by considering two resonance structures of the HBDI anion, see figure 2 from ref 4. The interaction between these two structures results in charge delocalization between two oxygen atoms and in scrambling CC bond orders as discussed, for example, in ref 23. The $C_{1P}-C_{1B}$ bond acquires a double-bond character, whereas the order of $C_{1B}-C_{1I}$ bond is reduced. Natural bond orbital (NBO)[40,41] charges and bond

Table 1. Geometry Parameters at the Stationary Points for the Gas-Phase *Cis*−*Trans* Chromophore Isomerization[a]

structure	method	C_{1P}−C_{1B}	C_{1B}−C_{1I}	τ_P	τ_I
cis-isomer	PBE0/6-31+G(d,p)	1.404	1.385	0	180
	CASSCF(12/11)/cc-pVDZ	1.406	1.383	0	180
	SOS-MP2/cc-pVDZ	1.415	1.397	0	180
	SA3-CAS(4,3)/DZP[b]	1.408	1.382	0	180
transition state	PBE0/6-31+G(d,p)	1.365	1.458	0.3	88.2
	CASSCF(12/11)/cc-pVDZ	1.362	1.477	1.0	86.4
	SOS-MP2/cc-pVDZ	1.374	1.476	0.0	87.6
trans-isomer	PBE0/6-31+G(d,p)	1.403	1.392	0	0
	CASSCF(12/11)/cc-pVDZ	1.402	1.395	0	0
	SOS-MP2/cc-pVDZ	1.414	1.405	0	0
	SA3-CAS(4/3)/DZP[b]	1.407	1.390	0	0

[a] Distances in Å and angles in degrees. [b] Ref 23.

Table 2. Cumulative Natural Charges on the Fragments of the HBDI molecule: the Phenyl and Dimethylimidazolin Rings and the CH bridge Calculated with CASSCF(12/11) and DFT (PBE0 Functional)

	CASSCF(12/11)/cc-pVDZ			PBE0/6-31+G(d,p)		
	cis	TS	*trans*	*cis*	TS	*trans*
			Gas Phase			
phenyl	−0.61	−0.20	−0.50	−0.59	−0.30	−0.57
bridge	0.13	0.13	0.11	0.10	0.20	0.09
imidazolin	−0.52	−0.93	−0.61	−0.51	−0.90	−0.52
			Solution[a]			
phenyl	−0.85	−0.09	−0.91	−0.63	−0.19	−0.70
bridge	0.14	0.08	0.11	0.13	0.16	0.13
imidazolin	−0.29	−0.99	−0.20	−0.50	−0.97	−0.43

[a] Calculated with QM/MM: EFP for the solvent−QM part interaction and TIP3P for the water−water interaction.

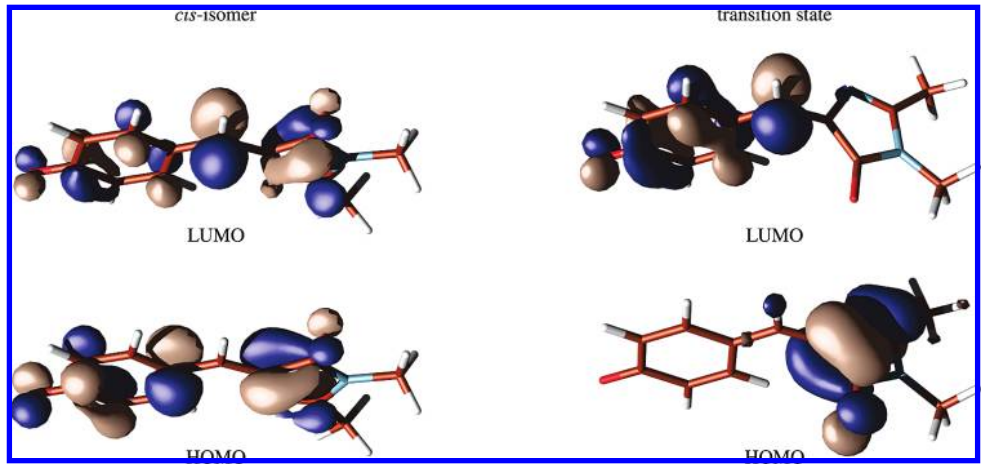

Figure 3. Frontier valence molecular orbitals of the HBDI anion in the *cis*-form (left) and at the transition state of the *cis*−*trans* isomerization path (right).

orders (see ref 4) are consistent with computed bond lengths. Overall, CASSCF slightly exaggerates bond alternation relative to DFT (or MP2, see ref 4) in favor of the canonical structure (Figure 1).

At the TS, the two rings are nearly perpendicular to each other ($\tau_I = 87-88°$), which disturbs the π system and breaks the resonance interaction. The bond alternation pattern is reversed such that C_{1P}−C_{1B} becomes shorter than C_{1B}−C_{1I}, suggesting that one of the two resonance structures becomes dominant. All the methods agree on the magnitude of the change relative to the equilibrium structures: C_{1P}−C_{1B}, which is longer at the *cis*- and *trans*-geometries, becomes shorter by about 0.04 Å at the TS, whereas the C_{1B}−C_{1I} bond is about 0.07 Å longer at the saddle point. NBO charges (Table 2) and the molecular orbital picture (Figure 3) reveal almost complete charge localization on the imidazolin ring.

Despite the similarity of the computed geometry parameters and charge distributions at the minima and the TS computed with DFT and CASSCF, respective activation energies differ by more than 10 kcal/mol (34.5 versus 22.5 kcal/mol). Note that the corresponding *cis*−*trans* energy differences are very close: 2.3 and 3.5 kcal/mol, respectively. A close inspection of the charges from Table 1 reveals slightly more polar charge distribution for the PBE0 density: the positive charge on the bridge moiety is 0.19 versus 0.13 at the CASSCF level. Because of the large energy penalty

Table 3. *Cis-Trans* Energy Difference ΔE_{tc} and the Energy Barrier E_a for the *Cis*−*Trans* Isomerization of the HBDI Anion Calculated at Various Levels of Theory for the Chromophore Molecule and Solvent

method		ΔE_{tc}, kcal/mol			E_a, kcal/mol		
chromophore	solvent	gas phase	solution	shift	gas phase	solution	shift
PBE0/6-31+G(d,p)		2.3			34.5		
	D-PCM		2.1	−0.2		33.5	−1.0
	C-PCM		2.3	+0.0		34.0	−0.5
	SVPE		2.1	−0.2		24.6	−9.9
	QM/MM[a]		5.0	+2.7		26.0	−8.5
CASSCF(12/11)/cc-pVDZ		3.5			22.5		
	SVPE		2.6	−0.9		9.9	−12.6
	QM/MM[a]		2.1	−1.4		11.1	−11.4
MRMP2/cc-pVDZ		3.7			26.2		

[a] Calculated with QM/MM: EFP for the solvent−QM part interaction and TIP3P for the water−water interaction.

due to charge separation in the gas phase, small differences in ionicity may produce a large effect. Another notable difference is larger asymmetry in oxygen charges: at the CASSCF level the imidazolin oxygen is by 0.22*e* more negative than that of the phenyl oxygen, whereas at the DFT level this difference is reduced to 0.15. This suggests a larger contribution of the second resonance structure in the CASSCF wave function, which can also contribute to the energy difference.

More ionic character of the PBE0 density and the cusp-like shape of the profile (Figure 2) are due to the multiconfigurational character of the wave function at the TS, which is not adequately described by DFT (or MP2). The CASSCF amplitudes show almost equal weights of the two dominant configurations, $(HOMO)^2$ and $(HOMO)^1(LUMO)^1$ at the TS. The HOMO and LUMO at the TS differ considerably from those at the equilibrium geometry (shown in figure 3 of ref 4), they become localized on the imidazolin and phenyl rings, respectively. Thus, $(HOMO)^2$ and $(LUMO)^2$ correspond to the two charge-localized configurations, and their interaction results in less ionic electron distribution. The ionicity is also reduced by $(HOMO)^1(LUMO)^1$.

A stability analysis of the Hartree−Fock wave function at the TS shows a RHF−UHF (restricted and unrestricted Hartree-Fock) instability with a negative eigenvalue of −0.037. The DFT/PBE0 solution, however, proves to be stable, which means that using the symmetry broken unrestricted solution to achieve better description of the barrier will not be useful in this case. Therefore, a multiconfigurational approach is necessary not only for describing excited-state isomerization of the GFP-like chromophores but also for modeling isomerization in the ground state.

Although the CASSCF wave function is capable of capturing the multiconfigurational character of the wave function, it needs to be augmented by dynamical correlation to provide accurate energy differences. We included dynamical correlation correction via MRMP2 for the E_{tc} and E_a energies (at the CASSCF geometries). This yields an activation energy of $E_a = 26.2$ kcal/mol, which is 3.7 kcal/mol higher than that of the CASSCF result.

The CASSCF results represent an improvement over DFT; however, there is still a considerable discrepancy between the theoretical (22−26 kcal/mol) and experimental (15.4 kcal/mol) values for E_a, as noted by the authors of experimental studies.[12,13,17] Below we demonstrate that this discrepancy is resolved when solvent effects are taken into account.

3.2. *Cis*−*Trans* Isomerization Pathway in Aqueous Solution: Continuum Solvation Models. Continuum solvation models[32] provide a reasonable starting point in modeling ground-state isomerization in aqueous solution. At first, two versions of the polarized continuum model (PCM), D-PCM[33] and C-PCM,[34] were applied to optimize the equilibrium geometry parameters of the *cis*- and *trans*-isomers and the TS configuration and to compute the relative energies ΔE_{tc} and E_a at the PBE0/6-31+G(d,p) level. Both models produced similar results: $\Delta E_{tc} = 2.1$ (D-PCM) and 2.3 kcal/mol (C-PCM); $E_a = 33.5$ (D-PCM) and 34.0 kcal/mol (C-PCM). The geometry parameters and the energies are close to the gas-phase values obtained with the same DFT model. These results are fairly stable with respect to the basis set: upon expanding it to 6-311++G(2d,p), E_a and ΔE_{tc} change by less than 1.5 and 0.7 kcal/mol, respectively. Table 3 summarizes solvent effects on E_{tc} and E_a computed using different approaches.

Next, we considered a new version of the continuum solvation model, SVPE,[35] which has recently been implemented in GAMESS(US),[29] for the single point calculations of relative energies ΔE_{tc} and E_a at the gas-phase geometry parameters. At the PBE0/6-31+G(d,p) level, we obtained a considerable reduction of the activation energy compared to the PCM results: $E_a = 24.6$ kcal/mol, while the energy $\Delta E_{tc} = 2.1$ kcal/mol was almost the same as in the PCM model. According to a comment by Chipman,[35] the improvements introduced in SVPE do affect the reaction barrier estimated with the continuum solvation models, especially for charged substrates. The large solvent effect on E_a (9.1 kcal/mol reduction relative to the gas-phase value) is consistent with the more ionic character of the TS (see Table 2).

Finally, we combined the SVPE model with the adequate description of the electronic structure of the solute and carried out the calculations of relative energies with the CASSCF(12/11)/cc-pVDZ description for the chromophore. The quantities, $\Delta E_{tc} = 2.6$ and $E_a = 9.9$ kcal/mol, can now be directly compared to the experimental free-energy difference of 2.3 and 15.4 kcal/mol.[12] The reduction of about 15 kcal/mol in E_a when going from DFT to CASSCF results within the SVPE solvation model is consistent with the corresponding reduction (13 kcal/mol) in the gas-phase calculations.

Moreover, DFT and CASSCF agree in the magnitude of the reduction of E_a due to solvent (9.1 and 12.6 kcal/mol, respectively). Thus, the absolute value of E_a is overestimated by DFT due to the multiconfigurational character of the electronic structure at the TS geometry, which is correctly captured by CASSCF.

3.3. *Cis*−*Trans* Isomerization Pathway in Aqueous Solution: Explicit Solvent Molecules. The relative energies ΔE_{tc} and E_a for the HBDI anion inside a cluster of water molecules were computed using a QM/MM technique. To build the starting point, the chromophore molecule at the gas-phase TS geometry was placed in a sphere of 200 water molecules using the VMD computer program.[42] After running short molecular dynamics trajectories at various temperatures, the energy was minimized using molecular mechanics with the CHARMM force field[43] by keeping the solute species frozen. Then the solvent outside the first solvation shell was removed with 49 water molecules completely covering the chromophore remaining in the system. This saddle point structure was reoptimized for all geometric degrees of freedom by QM/MM using DFT with the PBE0 functional and the 6-31+G(d,p) basis for the QM-part (chromophore), EFP[36] for QM-solvent interactions, and the empirical TIP3P potential for water−water interactions. The steepest descent pathways taken in both directions from the optimized TS lead to the *cis*- and *trans*-isomers of the trapped chromophore (Figure 4). The energies obtained with this method, ΔE_{tc} = 5.0 kcal/mol and E_a = 26.0 kcal/mol, are consistent with the DFT/SVPE calculations (Table 3).

The energies of the *cis*-, *trans*- and TS structures were also calculated using CASSCF(12/11) for in the QM-part. The interactions between the chromophore molecule and solvent and between the water molecules were handled with EFP and TIP3P, respectively. In line with the gas-phase and dielectric continuum model results, the activation energy is lower at the CASSCF level relative to those of DFT: ΔE_{tc} = 2.1 kcal/mol, E_a = 11.1 kcal/mol.

The relative energies can be further refined by including the dynamical correlation effects. In the gas phase, accounting for dynamical correlation via MRMP2 raises the CASSCF activation barrier by 3.7 kcal/mol. Applying that correction, we estimate the activation energy for the *cis*−*trans* isomerization of the GFP chromophore in aqueous solution to be 14.8 kcal/mol. The remaining discrepancy with the experimental value of 15.4 kcal/mol[12] can be partly attributed to the differences between the potential-energy and the free-energy barriers. The present QM/MM model with only 49 explicit water molecules is not sufficient for describing the statistical state in solution. This water solvation shell completely covers the chromophore molecule and accounts for principal environmental effects, but precise free-energy values, along the isomerization pathway, should be estimated by using more appropriate condensed-phase models. As shown, e.g., in ref 44, no considerable changes in conclusions are expected if the dielectric continuum model is applied on top of the model with explicit water molecules.

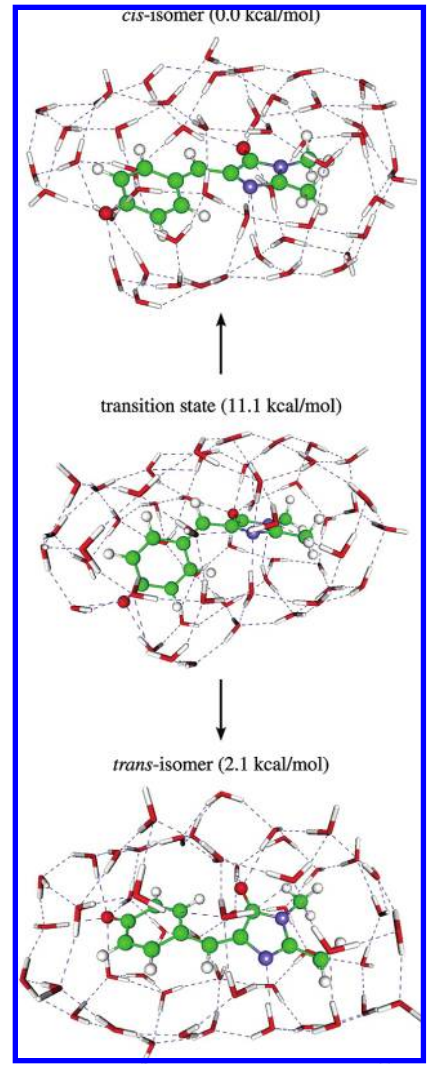

Figure 4. *Cis-trans* isomerization of the chromophore inside a cluster of water molecules. Relative energies of the stationary points are computed with QM(CASSCF(12/11)/cc-pVDZ)/EFP/MM(TIP3P).

4. Conclusion

Calculations of the *cis*−*trans* isomerization pathway require wave functions that are flexible enough to reflect the multiconfigurational character of the transition state. CASSCF gives a qualitatively correct curve, whereas DFT and SOS-MP2 fail at the twisted geometries. The gas-phase CASSCF value of the barrier height is 10 kcal/mol higher than that of the experimental value; however, the inclusion of solvent effects brings it down to 9.9−11.1 kcal/mol, which agrees well with 15.4 kcal/mol derived from experimental measurements. Including dynamical correlation correction yields 14.8 kcal/mol, which is within 0.8 kcal/mol from the experiment. Good agreement between SVPE and QM/MM calculations further supports the validity of our results. A large solvent effect on E_a is due to the more ionic character of the TS, where the negative charge is localized on imidazolin ring, which is in contrast to the equilibrium structure, where the negative charge is delocalized between the two rings. Our calculations help to resolve previous

disagreements between theory and experiment with respect to the GFP chromophore isomerization in an aqueous solution.

Acknowledgment. We thank Alex Granovsky for generous help and valuable discussions of this work. This work is supported by the joint grant from the U.S. Civilian Research and Development Foundation (project RUC1-2914-MO-07) and the Russian Foundation for Basic Research (08-03-91104-AFGIR). I.P., B.G., and A.N. thank the SKIF-GRID program and SKIF-Siberia for providing computational resources. E.E. and A.I.K. acknowledge the iOpenShell Center for Computational Studies of Electronic Structure and Spectroscopy of Open-Shell and Electronically Excited Species (http://iopenshell.usc.edu) supported by the National Science Foundation through the CRIF:CRF CHE-0625419 + 0624602 + 0625237 grant as well as through the CHE-0616271 grant (AIK). A.I.K. is grateful to the Institute of Mathematics and its Applications in Minnesota for its hospitality and productive environment during her stay as a visiting professor.

Supporting Information Available: Optimized geometry of the HBDI anion and the anion in water, the natural population analysis, the imaginary frequency mode at the TS, and the CASSCF natural orbitals figures. This material is available free of charge via the Internet at http://pubs.acs.org.

References

(1) Tsien, R. Y. *Annu. Rev. Biochem.* **1998**, *67*, 509.

(2) Zimmer, M. *Chem. Rev.* **2002**, *102*, 759.

(3) Stepanenko, O. V.; Verkhusha, V. V.; Kuznetsova, I. M.; Uversky, V. N.; Turoverov, K. K. *Curr. Protein Pept. Sci.* **2008**, *9*, 338.

(4) Epifanovsky, E.; Polyakov, I.; Grigorenko, B. L.; Nemukhin, A. V.; Krylov, A. I. *J. Chem. Theory Comput.* 2009; DOI: 10.1021/ct903187f.

(5) Henderson, J. N.; Remington, S. J. *Physiology* **2006**, *21*, 162.

(6) Chen, R. F. *Arch. Biochem. Biophys.* **1977**, *179*, 672.

(7) Steiner, R. F.; Albaugh, S.; Nenortas, E.; Norris, L. *Biopolymers* **1997**, *32*, 73.

(8) Babendure, J. R.; Adams, S. R.; Tsien, R. Y. *J. Am. Chem. Soc.* **2003**, *125*, 14716.

(9) Silva, G. L.; Ediz, V.; Yaron, D.; Armitage, B. A. *J. Am. Chem. Soc.* **2007**, *129*, 5710.

(10) Constantin, T. P.; Silva, G. L.; Robertson, K. L.; Hamilton, T. P.; Fague, K.; Waggoner, A. S.; Armitage, B. A. *Org. Lett.* **2008**, *10*, 1561.

(11) Özhalici-Ünal, H.; Pow, C. L.; Marks, S. A.; Jesper, L. D.; Silva, G. L.; Shank, N. I.; Jones, E. W.; Burnette, J. M.; Berget, P. B.; Armitage, B. A. *J. Am. Chem. Soc.* **2008**, *130*, 1260.

(12) He, X.; Bell, A. F.; Tonge, P. J. *FEBS Lett.* **2003**, *549*, 35.

(13) Hager, B.; Schwarzinger, B.; Falk, H. *Monatsh. Chem.* **2006**, *137*, 163.

(14) Loos, D. C.; Habuchi, S.; Flors, C.; Hotta, J.; Wiedenmann, J.; Nienhaus, G. U.; Hofkens, J. *J. Am. Chem. Soc.* **2006**, *128*, 6270.

(15) Yang, J.-S.; Huang, G.-J.; Liu, Yi.-H.; Peng, S.-M. *Chem. Commun.* **2008**, 1344.

(16) Nienhaus, K.; Nar, H.; Heiker, R.; Wiedenmann, J.; Nienhaus, G. U. *J. Am. Chem. Soc.* **2008**, *130*, 12578.

(17) Dong, J.; Abulwerdi, F.; Baldridge, A.; Kowalik, J.; Solntsev, K. M.; Tolbert, L. M. *J. Am. Chem. Soc.* **2008**, *130*, 14096.

(18) Voityuk, A. A.; Michel-Beyerle, M.-E.; Rösch, N. *Chem. Phys. Lett.* **1997**, *272*, 162.

(19) Weber, W.; Helms, V. J. A.; McCammon; Langhoff, P. W. *Proc. Nat. Acad. Sci. U.S.A.* **1999**, *96*, 6177.

(20) Levine, B. G.; Martinez, T. J. *Annu. Rev. Phys. Chem.* **2007**, *58*, 613.

(21) Schäfer, L. V.; Groenhof, G.; Klingen, A. R.; Ullmann, G. M.; Boggio-Pasqua, M.; Robb, M. A.; Grubmüller, H. *Angew. Chem., Int. Ed.* **2007**, *119*, 536.

(22) Schäfer, L. V.; Groenhof, G.; Boggio-Pasqua, M.; Robb, M. A.; Grubmüller, H. *PLoS Comput. Biol.* **2008**, *4*, e1000034.

(23) Olsen, S.; Smith, S. C. *J. Am. Chem. Soc.* **2008**, *130*, 8677.

(24) Andresen, M.; Wahl, M. C.; Stiel, A. C.; Gräter, F.; Schäfer, L. V.; Trowitzsch, S.; Weber, G.; Eggeling, C.; Grubmüller, H.; Hell, S. W.; Jakobs, S. *Proc. Nat. Acad. Sci. U.S.A.* **2005**, *102*, 13070.

(25) Adamo, C.; Barone, V. *J. Chem. Phys.* **1999**, *110*, 6158.

(26) Perdew, J. P.; Burke, K.; Ernzerhof, M. *Phys. Rev. B: Condens. Matter Mater. Phys.* **1996**, *77*, 3865.

(27) Dunning, T. H. *J. Chem. Phys.* **1989**, *90*, 1007.

(28) Granovsky, A. *PC GAMESS*. http://classic.chem.msu.su/gran/gamess/index.html (accessed April 27, 2009).

(29) Schmidt, M. W.; Baldridge, K. K. J. A.; Boatz, S. T.; Elbert; Gordon, M. S.; J. H.; Jensen, S.; Koseki; Mastunaga, N.; Nguyen, K. A. S.; Su, T. L.; Windus; Dupuis, M.; Montgomery, J. A. *J. Comput. Chem.* **1993**, *14*, 1347.

(30) Shao, Y.; Molnar, L. F.; Jung, Y.; Kussmann, J.; Ochsenfeld, C.; Brown, S.; Gilbert, A. T. B.; Slipchenko, L. V.; Levchenko, S. V.; O'Neil, D. P.; Distasio, R. A. R. C., Jr.; Lochan, Wang, T.; Beran, G. J. O.; Besley, N. A.; Herbert, J. M.; Lin, C. Y.; Van Voorhis, T.; Chien, S. H.; Sodt, A.; Steele, R. P.; Rassolov, V. A.; Maslen, P.; Korambath, P. P.; Adamson, R. D.; Austin, B.; Baker, J.; Bird, E. F. C.; Daschel, H.; Doerksen, R. J.; Drew, A.; Dunietz, B. D.; Dutoi, A. D.; Furlani, T. R.; Gwaltney, S. R.; Heyden, A.; Hirata, S.; Hsu, C.-P.; Kedziora, G. S.; Khalliulin, R. Z.; Klunziger, P.; Lee, A. M.; Liang, W. Z.; Lotan, I.; Nair, N.; Peters, B.; Proynov, E. I.; Pieniazek, P. A.; Rhee, Y. M.; Ritchie, J.; Rosta, E.; Sherrill, C. D.; Simmonett, A. C.; Subotnik, J. E.; Woodcock, H. L.; Zhang, W.; Bell, A. T.; Chakraborty, A. K.; Chipman, D. M.; Keil, F. J.; Warshel, A.; Herhe, W. J.; Schaefer, H. F.; Kong, J.; Krylov, A. I.; Gill, P. M. W.; Head-Gordon, M. *Phys. Chem. Chem. Phys.* **2006**, *8*, 3172.

(31) Ponder, J. W. *TINKER*−*Software Tools for Molecular Design*. http://dasher.wustl.edu/tinker/ (accessed May 7, 2009).

(32) Tomasi, J.; Mennucci, B.; Cammi, R. *Chem. Rev.* **2005**, *105*, 2999.

(33) Cossi, M.; Barone, V. *J. Chem. Phys.* **1998**, *109*, 6246.

(34) Barone, V.; Cossi, M. *J. Phys. Chem. A* **1998**, *102*, 1995.

(35) Chipman, D. M. *J. Chem. Phys.* **2006**, *124*, 224111.

(36) Gordon, M. S.; Freitag, M. A.; Bandyopadhyay, P.; Jensen, J. H.; Kairys, V.; Stevens, W. J. *J. Phys. Chem. A* **2001**, *105*, 293.

(37) Adamovic, I.; Freitag, M. A.; Gordon, M. S. *J. Chem. Phys.* **2003**, *118*, 6725.

(38) Nemukhin, A. V.; Grigorenko, B. L.; Topol, I. A.; Burt, S. K. *Phys. Chem. Chem. Phys.* **2004**, *6*, 1031.

(39) Grigorenko, B. L.; Rogov, A. V.; Nemukhin, A. V. *J. Phys. Chem. B* **2006**, *110*, 4407.

(40) Weinhold, F.; Landis, C. R. *Chem. Edu.: Res. Pract. Eur.* **2001**, *2*, 91.

(41) NBO 5.0. Glendening, E. D.; Badenhoop, J. K.; Reed, A. E.; Carpenter, J. E.; Bohmann, J. A.; Morales, C. M.; Weinhold, F. *NBO 5.0*; Theoretical Chemistry Institute, University of Wisconsin: Madison, WI, 2001.

(42) Humphrey, W.; Dalke, A.; Schulten, K. *J. Mol. Graphics* **1996**, *14*, 33.

(43) Brooks, B. R.; Bruccoleri, R. E.; Olafson, B. D.; States, D. S.; Swaminathan, S.; Karplus, M. *J. Comput. Chem.* **1983**, *4*, 187.

(44) Nemukhin, A. V.; Topol, I. A.; Burt, S. K. *J. Chem. Theory Comput.* **2006**, *2*, 292.

CT9001448